

DTIC FILE COPY

4

TECHNICAL REPORT BRL-TR-2958  
(SUPERSEDES IMR-904)

**BRL**

1938 - Serving the Army for Fifty Years - 1988

AD-A202 414

COMPUTATIONAL FLUID DYNAMICS CAPABILITY  
FOR THE SOLID FUEL RAMJET PROJECTILE

MICHAEL J. NUSCA  
SUKUMAR R. CHAKRAVARTHY  
URIEL C. GOLDBERG

DECEMBER 1988

DTIC  
ELECTE  
JAN 12 1989  
S H D

APPROVED FOR PUBLIC RELEASE; DISTRIBUTION UNLIMITED.

U.S. ARMY LABORATORY COMMAND

**BALLISTIC RESEARCH LABORATORY  
ABERDEEN PROVING GROUND, MARYLAND**

89 1 12 021

DESTRUCTION NOTICE

Destroy this report when it is no longer needed. DO NOT return it to the originator.

Additional copies of this report may be obtained from the National Technical Information Service, U.S. Department of Commerce, Springfield, VA 22161.

The findings of this report are not to be construed as an official Department of the Army position, unless so designated by other authorized documents.

The use of trade names or manufacturers' names in this report does not constitute indorsement of any commercial product.

UNCLASSIFIED

SECURITY CLASSIFICATION OF THIS PAGE

## REPORT DOCUMENTATION PAGE

Form Approved  
OMB No. 0704-0188

1a. REPORT SECURITY CLASSIFICATION <b>UNCLASSIFIED</b>			1b. RESTRICTIVE MARKINGS		
2a. SECURITY CLASSIFICATION AUTHORITY			3. DISTRIBUTION/AVAILABILITY OF REPORT Approved for public release; distribution is unlimited.		
2b. DECLASSIFICATION/DOWNGRADING SCHEDULE			4. PERFORMING ORGANIZATION REPORT NUMBER(S) BRL-TR-2958		
4. PERFORMING ORGANIZATION REPORT NUMBER(S) BRL-TR-2958			5. MONITORING ORGANIZATION REPORT NUMBER(S)		
6a. NAME OF PERFORMING ORGANIZATION U.S. Army Ballistic Research Laboratory		6b. OFFICE SYMBOL (If applicable) SLCBR-LF	7a. NAME OF MONITORING ORGANIZATION		
6c. ADDRESS (City, State, and ZIP Code) Aberdeen Proving Ground, MD 21005-5066			7b. ADDRESS (City, State, and ZIP Code)		
8a. NAME OF FUNDING/SPONSORING ORGANIZATION U.S. Army Ballistic Research Laboratory		8b. OFFICE SYMBOL (If applicable) SLCBR-DD-T	9. PROCUREMENT INSTRUMENT IDENTIFICATION NUMBER		
8c. ADDRESS (City, State, and ZIP Code) Aberdeen Proving Ground, MD 21005-5066			10. SOURCE OF FUNDING NUMBERS		
			PROGRAM ELEMENT NO 62618A	PROJECT NO. 1L1 62618AH80	TASK NO.
					WORK UNIT ACCESSION NO.
11. TITLE (Include Security Classification) Computational Fluid Dynamics Capability for the Solid Fuel Ramjet Projectile (U)					
12. PERSONAL AUTHOR(S) Nusca, Michael J.; Chakravarthy, Sukumar R.; and Goldberg, Uriel C.					
13a. TYPE OF REPORT Technical Report		13b. TIME COVERED FROM _____ TO _____		14. DATE OF REPORT (Year, Month, Day) 1988 August	15. PAGE COUNT 28
16. SUPPLEMENTARY NOTATION Supersedes BRL-IMR-904 dated January 1988.					
17. COSATI CODES			18. SUBJECT TERMS (Continue on reverse if necessary and identify by block number)		
FIELD	GROUP	SUB-GROUP	Solid-Fuel Ramjet; Computational Fluid Dynamics		
01	01		Tubular Projectiles; TVD Scheme		
21	08.2		Navier-Stokes; Separated Flow.		
19. ABSTRACT (Continue on reverse if necessary and identify by block number) A computational fluid dynamics solution of the Navier-Stokes equations has been applied to the internal and external flow of inert solid-fuel ramjet projectiles. Computational modeling reveals internal flowfield details not attainable by flight or wind tunnel measurements, thus contributing to the current investigation into the flight performance of solid-fuel ramjet projectiles. The present code employs numerical algorithms termed total variational diminishing (TVD). Computational solutions indicate the importance of several special features of the code including the zonal grid framework, the TVD scheme, and a recently developed backflow turbulence model. The solutions are compared with results of internal surface pressure measurements. As demonstrated by these comparisons, the use of a backflow turbulence model distinguishes between satisfactory and poor flowfield predictions.					
20. DISTRIBUTION/AVAILABILITY OF ABSTRACT <input type="checkbox"/> UNCLASSIFIED/UNLIMITED <input checked="" type="checkbox"/> SAME AS RPT <input type="checkbox"/> DTIC USERS			21. ABSTRACT SECURITY CLASSIFICATION UNCLASSIFIED		
22a. NAME OF RESPONSIBLE INDIVIDUAL Michael J. Nusca			22b. TELEPHONE (Include Area Code) (301)-278-2057	22c. OFFICE SYMBOL SLCBR-LF-A	

## Table of Contents

	<u>Page</u>
List of Figures . . . . .	v
I. INTRODUCTION . . . . .	1
II. COMPUTATIONAL APPROACH . . . . .	3
1. EQUATIONS OF MOTION. . . . .	3
2. TURBULENCE MODELING. . . . .	4
3. COMPUTATIONAL ALGORITHM. . . . .	5
4. COMPUTATIONAL GRID. . . . .	6
III. RESULTS . . . . .	7
1. IMPORTANCE OF FLOW TRANSITION AND TURBULENCE. . . . .	8
2. DISCUSSION OF COMPUTED RESULTS. . . . .	9
IV. CONCLUSIONS . . . . .	10
REFERENCES . . . . .	23
DISTRIBUTION LIST . . . . .	25



Accession For	
NTIS GRA&I	<input checked="" type="checkbox"/>
DTIC TAB	<input type="checkbox"/>
Unannounced	<input type="checkbox"/>
Justification	
By _____	
Distribution/	
Availability Codes	
Dist	Avail and/or Special
<b>A-1</b>	

## List of Figures

<u>Figure</u>		<u>Page</u>
1	SFRJ Geometry; Dimensions in Millimeters, $D_{inj}=43.2, 48.3\text{mm}$ (1.7, 1.9 Inches), $D_{nt}=27.9, 39.7, 40.6\text{ mm}$ (1.1, 1.564, 1.6 Inches). . . . .	12
2	Zone Designations for Axisymmetric SFRJ Geometry. Dimensions in Inches. 1: Inlet; 2: Injector; 3: Combustion Section; 4: Nozzle; 5: Base; 6: Exterior. . . . .	13
3	Computational Grid for Axisymmetric SFRJ. Dimensions in Inches (Nearfield Shown). . . . .	14
4	Internal Surface Pressure Distribution for SFRJ, $M_{\infty}=4.03$ , 1.7 in. Injector, 1.6 in. Nozzle. Effect of Viscous Modeling. . . . .	15
5	Internal Surface Pressure Distribution for SFRJ, $M_{\infty}=4.03$ , 1.7 in. Injector, 1.6 in. Nozzle. Effect of Flow Transition Location. . . . .	16
6	Internal Surface Pressure Distribution for SFRJ, $M_{\infty}=4.03$ , 1.9 in. Injector, 1.1 in. Nozzle. Effect of Flow Transition Location. . . . .	17
7	Internal Surface Pressure Distribution for SFRJ, $M_{\infty}=4.03$ . 1.7 in. Injector, 1.1, 1.54, and 1.6 in. Nozzles. . . . .	18
8	Pressure Contours for SFRJ, $M_{\infty}=4.03$ , 1.7 in. Injector, 1.6 in. Nozzle. Dimensions in Inches. . . . .	19
9	Pressure Contours for SFRJ, $M_{\infty}=4.03$ , 1.7 in. Injector, 1.1 in. Nozzle. Dimensions in Inches. . . . .	20
10	Internal Surface Pressure Distribution for SFRJ, $M_{\infty}=4.03$ . 1.9 in. Injector, 1.1, 1.54, and 1.6 in. Nozzles. . . . .	21

# I. INTRODUCTION

Various solid-fuel, tubular ramjet projectiles have been developed at the U.S. Army Ballistic Research Laboratory (BRL).<sup>1,2</sup> One of these projectiles has been designed for use as a tank gun training round (TGTR) for the 105mm, M68 tank cannon. The goal of the program is to demonstrate a TGTR of low dispersion at three kilometers and a maximum (safety) range of eight kilometers. The concept of the TGTR is to use the thrust (hence low drag) of the solid-fuel ramjet (SFRJ) projectile to obtain a ballistic match with low drag kinetic energy projectiles up to three kilometers. Upon depletion of the solid propellant and choking of the internal flow, the SFRJ will become a high-drag projectile with limited range. The successful demonstration of the SFRJ projectile has included the verification of flight and motor performance, limited safety range and ballistic match to a kinetic energy projectile up to 2.5 kilometers with somewhat higher dispersion than desired. Investigations into the combustion efficiency are currently under way in an effort to extend the ballistic match to 3 kilometers. Computational flow modeling significantly contributes to this investigation by adding to the current understanding of the SFRJ internal flow.

Computational modeling of the internal and external flow for a 75mm SFRJ projectile has been under way at the BRL Launch and Flight Division in recent years. A computational fluid dynamics (CFD) code utilizing an implicit, factored, time-stepping algorithm in a zonal grid framework has been developed by Chakravarthy.<sup>3</sup> This code employs a class of numerical algorithms, termed total variational diminishing or TVD, which do not require the inclusion of smoothing or dissipation functions to achieve numerical stability. The code can be used in conjunction with various turbulence and separated flow modeling techniques. Modeling strategies investigated include: a) the Baldwin-Lomax turbulence model<sup>4</sup> applied throughout the flowfield; b) the Baldwin-Lomax model applied outside of backflow regions, and the backflow turbulence model of Goldberg<sup>5</sup> applied within these regions. This code has been previously employed in the solution of subsonic, transonic, supersonic and mixed flow problems including complex supersonic inlet and nozzle flows

<sup>1</sup> Mermagen W.H., Yalamanchili R.J., "First Diagnostic Tests of a 75mm Solid Fuel Ramjet Tubular Projectile," US Army Ballistic Research Laboratory, Aberdeen Proving Ground, Maryland, ARBRL-09263, June 1983. (AD A130596)

<sup>2</sup> Mermagen W.H., Yalamanchili R.J., "Experimental Tests of a 105/75mm Solid Fuel Ramjet Tubular Projectile," US Army Ballistic Research Laboratory, Aberdeen Proving Ground, Maryland, ARBRL-MR-3416, December 1984. (AD B089766)

<sup>3</sup> Chakravarthy, S.R. "A New Computational Capability for Ramjet Projectiles," ARBRL-CR-595, U.S. Army Ballistic Research Laboratory, Aberdeen Proving Ground, MD, March 1988. (Also Goldberg, U., Chakravarthy, S., and Nusca, M., AIAA-87-2411, Proceedings of the 14th AIAA Atmospheric Flight Mechanics Conference, Monterey, CA, August 17-19, 1987.)

<sup>4</sup> Baldwin, B.S. and Lomax, H., "Thin Layer Approximation and Algebraic Model for Separated Turbulent Flows," AIAA-78-257, Proceedings of the 16th AIAA Aerospace Sciences Meeting, Huntsville, AL, January 16-18, 1976.

<sup>5</sup> Goldberg U.C., "Separated Flow Treatment with a New Turbulence Model," *AIAA Journal*, Vol. 24, No. 10, October 1986, pp. 1711-1713.

by Chakravarthy et. al.<sup>6-11</sup> This report describes application of the code to an inert SFRJ projectile. Results for axisymmetric (zero yaw) cold flow (no combustion or mass injection) are presented.

Previous computational efforts include the application of an unsteady, thin-layer Navier-Stokes code to ramjet type configurations<sup>12</sup> and an axisymmetric method of characteristics solution for ramjet inlet flow.<sup>13</sup> The latter solution assumed separated flow in the inlet and an experimentally determined inlet pressure level.

The SFRJ flight vehicle had a 1.7 inch diameter injector and a 1.54 inch diameter nozzle. During wind tunnel tests, small changes in total pressure produced dramatically different internal wall pressure distributions that were not observed for other injector/nozzle diameter combinations.<sup>14,15</sup> This unusual behavior could reflect bistable flow or highly complex flow states for this configuration. Comparisons between computed and measured internal wall pressures are made for several injector/nozzle diameter combinations and a single total pressure for which stable wall static pressures were observed. The detailed analysis of the effect of different total pressures for the 1.7/1.54 combination is not addressed in this report.

Cold flow, zero-yaw computations, for which internal flow measurements exist, are a necessary prelude to further extensions of the computational analysis for the SFRJ projectile. The zonal gridding approach of the code allows incorporation of a combustion model, such as that described by Vos,<sup>16</sup> into the combustion section of the internal geometry. After testing and validation, these reacting flow computations can be extended to the three-dimensional case, non-zero yaw, with direct comparisons with measured aerodynamic drag.

<sup>6</sup> Chakravarthy S.R., Szema K.Y., Goldberg U.C., Gorski J.J. (Rockwell International Science Center) and Osher S. (University of California). "Application of a New Class of High Accuracy TVD Schemes to the Navier-Stokes Equations," AIAA-85-0165, Proceedings of the 29th AIAA Aerospace Sciences Meeting, Reno NV., January 14-17, 1985.

<sup>7</sup> Chakravarthy S.R., Szema K.Y., "An Euler Solver for Three-Dimensional Supersonic Flows with Subsonic Pockets," AIAA-85-1703, Proceedings of the 18th AIAA Fluid Dynamics and Plasmadynamics and Lasers Conference, Cincinnati OH., July 16-18, 1985.

<sup>8</sup> Chakravarthy S.R., "The Versatility and Reliability of Euler Solvers Based on High-Accuracy TVD Formulations," AIAA-86-0243, Proceedings of the 24th AIAA Aerospace Sciences Meeting, Reno NV., January 6-9, 1986.

<sup>9</sup> Chakravarthy S.R., Harten A., Osher S., "Essentially Non-Oscillatory Shock-Capturing Schemes of Arbitrarily-High Accuracy," AIAA-86-0339, Proceedings of the 24th AIAA Aerospace Sciences Meeting, Reno NV., January 6-9, 1986.

<sup>10</sup> Sovo G.J., "Application of Navier-Stokes Analysis to Predict the Internal Performance of Thrust Vectoring Two-Dimensional Convergent-Divergent Nozzles," AIAA-88-2586, Proceedings of the 6th AIAA Applied Aerodynamics Conference, Williamsburg, VA, June 6-8, 1988.

<sup>11</sup> Chakravarthy, S.R., K.-Y. Szema, and Haney, J.W., "Unified "Nose-to-Tail" Computational Method for Hypersonic Vehicle Applications," AIAA-88-2564, Proceedings of the 6th AIAA Applied Aerodynamics Conference, Williamsburg, VA, June 6-8, 1988.

<sup>12</sup> Nietubicz, C.J., and Heavey, K.R., "Computational Flow Field Predictions for Ramjet and Tubular Projectiles," Proceedings of the 8th ADPA International Symposium on Ballistics, Orlando, FL, October 23-25, 1984.

<sup>13</sup> Danberg, J.E., and Sigal, A., "Evaluation of Solid Fuel Ramjet Projectile Aerodynamic Characteristics," Proceedings of the 10th ADPA International Symposium on Ballistics, San Diego, CA, October 27-29, 1987.

<sup>14</sup> Kayser L.D., Yalamanchili R.J., Trezler C., "Pressure Measurements on the Interior Surface of a 75mm Tubular Projectile at Mach 4," US Army Ballistic Research Laboratory, Aberdeen Proving Ground, Maryland, report in preparation.

<sup>15</sup> Yalamanchili R.J., unpublished wind tunnel data for the 75mm Tubular Projectile at Mach 4, US Army Ballistic Research Laboratory, Aberdeen Proving Ground, Maryland.

<sup>16</sup> Vos, J.B., "Calculating Turbulent Reacting Flows Using Finite Chemical Kinetics," *AIAA Journal*, Vol. 25, No. 10, October 1987, pp.1365-1372.

## II. COMPUTATIONAL APPROACH

The present CFD approach can be used to predict the compressible flowfield in and around an aerodynamic projectile by solving the 3D Navier-Stokes equations. At present only axisymmetric (zero yaw) flows have been investigated. These equations are solved with the assumption that the flow medium is air behaving as a perfect gas and that no chemical reactions are occurring. As a result only inert SFRJ projectiles are addressed at present. Both laminar and turbulent flows are investigated, thus an adequate turbulence model is required for closure. In addition, backflow regions can be present, thus a backflow turbulence model is included. The equations are transformed into conservation law form and discretized using finite volume approximations and the TVD formulation. The resulting set of equations is solved using an implicit, factored, time-stepping algorithm. This solution takes place on a computational grid that is generated around the projectile in zones where the zonal boundaries can be made transparent to the flowfield calculation.

### 1. EQUATIONS OF MOTION.

The compressible, Reynolds-averaged Navier-Stokes equations for 2D/axisymmetric flow are written in the following conservation form. The dependent variables  $u$ ,  $v$  and  $e$  are mass-averaged, with  $e$  being the specific total internal energy,  $T$  being temperature,  $\rho$  and  $p$  being the mean density and pressure, respectively, and  $t$  being time.

$$\frac{\partial W}{\partial t} + \frac{\partial F}{\partial x} + \frac{\partial G}{\partial y} + \left( \frac{G}{y} - \frac{H}{y} \right) \alpha = 0 \quad (1)$$

$$W = \begin{pmatrix} \rho \\ \rho u \\ \rho v \\ \rho e \end{pmatrix}, F = \begin{pmatrix} \rho u \\ \rho u^2 - \sigma_{xx} \\ \rho uv - \tau_{xr} \\ \rho ue + \dot{q}_x - \sigma_{xx}u - \tau_{xr}v \end{pmatrix}, G = \begin{pmatrix} \rho v \\ \rho uv - \tau_{xr} \\ \rho v^2 - \sigma_{rr} \\ \rho ve + \dot{q}_r - \tau_{xr}u - \sigma_{rr}v \end{pmatrix}$$

$$H = \begin{pmatrix} 0 \\ 0 \\ -\sigma_+ \\ 0 \end{pmatrix}$$

$$\sigma_{xx} = -p - \frac{2}{3}(\mu + \mu_t)\nabla \cdot U + 2(\mu + \mu_t)\frac{\partial u}{\partial x} \quad (2)$$

$$\sigma_{rr} = -p - \frac{2}{3}(\mu + \mu_t)\nabla \cdot U + 2(\mu + \mu_t)\frac{\partial v}{\partial y} \quad (3)$$

$$\sigma_+ = -p - \frac{2}{3}(\mu + \mu_t)\nabla \cdot U + 2(\mu + \mu_t)\frac{v}{y}\alpha \quad (4)$$

$$\tau_{rx} = \tau_{xr} = (\mu + \mu_t) \left( \frac{\partial u}{\partial y} + \frac{\partial v}{\partial x} \right) \quad (5)$$

$$\dot{q}_x = -C_p \left( \frac{\mu}{Pr} + \frac{\mu_t}{Pr_t} \right) \frac{\partial T}{\partial x} \quad (6)$$

$$\dot{q}_r = -C_p \left( \frac{\mu}{Pr} + \frac{\mu_t}{Pr_t} \right) \frac{\partial T}{\partial y} \quad (7)$$

$$e = C_v T + \frac{1}{2}(u^2 + v^2) \quad (8)$$

$$\nabla \cdot U = \frac{\partial u}{\partial x} + \frac{\partial v}{\partial y} + \frac{v}{y} \alpha \quad (9)$$

where  $\alpha = 1$  for axisymmetric flow and 0 for two dimensional flow.

In Equations 2-7, the laminar and eddy viscosities,  $\mu$  and  $\mu_t$ , are implicitly divided by the reference Reynolds number. The equations used for the Euler (inviscid) calculations are obtained from Equations 1-9 by setting both laminar and eddy viscosities to zero. In all calculations, the flow medium (air) was assumed to be a perfect gas, satisfying the equation of state

$$p = \rho RT \quad (10)$$

The following power law was used to relate molecular viscosity to temperature:<sup>17</sup>

$$\frac{\mu}{\mu_o} = \left( \frac{T}{T_o} \right)^n \quad (11)$$

where  $\mu_o = 0.1716$  mP,  $T_o = 491.6$  R, and  $n = 0.64874$ . The laminar and turbulent Prandtl numbers,  $Pr$  and  $Pr_t$ , were assumed constant with values of 0.72 and 0.9 respectively. The ratio of specific heats,  $\gamma$ , was also assumed constant and equal to 1.4. The specific heat capacities at constant volume and pressure,  $C_v$  and  $C_p$ , are related as  $\gamma = C_p/C_v$ .

In the  $\xi - \eta$  computational plane, Equation 1 is transformed into the finite volume conservation law form represented by<sup>6</sup>

$$\frac{\partial W}{\partial \tau} + \frac{1}{\text{Area}} \left( (y_\eta F - x_\eta G)_\xi + (-y_\xi F + x_\xi G)_\eta + \frac{G}{y} - \frac{H}{y} \right) = 0 \quad (12)$$

where  $\xi$  and  $\eta$  are the new independent variables and  $x_\xi$ ,  $x_\eta$ ,  $y_\xi$ , and  $y_\eta$  are the four transformation coefficients obtained numerically from the mapping procedure. The "Area" in Equation 12 denotes the area of the finite volume cell under consideration at the time of discretization of the equations. The transformed time variable is represented by  $\tau$ .

## 2. TURBULENCE MODELING.

The internal flowfield of the SFRJ projectile can include large regions of recirculatory flow, induced by both shock waves and by sharp geometrical discontinuities. Indeed internal surface pressure measurements made on an instrumented SFRJ wind tunnel model (unfueled) indicate that such regions do exist in the inlet and combustion sections.<sup>14,15</sup> Good modeling of these regions is critical to the overall flowfield solution quality. However most existing turbulence models either do not treat such regions or do so in an ad hoc fashion that is frequently inadequate. A notably different approach is the use of a full Reynolds stress closure model, involving the solution of five coupled partial differential

<sup>17</sup> Mazor G., Ben-Dor G., and Igra O., "A Simple and Accurate Expression for the Viscosity of Nonpolar Diatomic Gases up to 10,000 K," *AIAA Journal*, Vol. 23, No. 4, April 1985, pp. 636-638.

equations (for two-dimensional flows) for the three normal stresses, the shear stress, and the length scale. These must be supplemented by a wall function to provide turbulence quantities across viscous regions adjacent to solid surfaces. Such a wall function is usually some form of the law-of-the-wall, which, according to experimental observations, does not apply to detached flows. Thus, an expensive and time consuming computation of the Reynolds stresses is coupled with a questionable near-wall formulation.

To improve the predictive capability of separated flows using current Reynolds-averaged Navier-Stokes codes, a new turbulence model has been recently developed.<sup>5</sup> The new turbulence model is based on experimental observations of detached flows. The model prescribes turbulence kinetic energy ( $k$ ) and its dissipation ( $\epsilon$ ) analytically within backflows. A Gaussian variation of  $k$  normal to walls is assumed. The length scale of turbulence is proportional to the local distance from the wall to the edge of the viscous sublayer, which is located outside the backflow region. The latter feature is a basic assumption of the model. The stress scale is the local maximum Reynolds stress, which typically occurs around the middle of the boundary layer, well outside the separation bubble. This scale must be supplied by a turbulence model that is used beyond backflow regions.

The main equations of the backflow model are given in Reference 5. A formula for the eddy viscosity distribution within backflows results and is used to supply eddy viscosity for the Reynolds-averaged equations when the calculations are done inside separation bubbles. Outside of them, another turbulence model (for example Baldwin-Lomax<sup>4</sup>) supplies the values of eddy viscosity. While the Baldwin-Lomax turbulence model is used to detect flow separation and to initiate application of the backflow model, the latter model may relocate the separation point (and the reattachment point, if one exists). The location of flow separation as predicted by the Baldwin-Lomax turbulence model and Goldberg's backflow model are significantly different for the applications reported in Reference 18. For further details of how the model treats the influence of large eddies residing outside detached regions, the history effect of these eddies downstream of reattachment, and the mutual influence of multiple walls on the eddy viscosity, see Reference 18. The model has been tested successfully for a variety of flow conditions and body geometries including a backward-facing step in subsonic flow,<sup>18</sup> an axisymmetric bump in transonic flow,<sup>18</sup> and an axisymmetric boattail in transonic flow.<sup>19</sup>

### 3. COMPUTATIONAL ALGORITHM.

The spacial discretization technique for the equations of motion must be reliable and robust if it is to successfully capture the complex physics of SFRJ internal and external flowfields. The TVD formulation for the convection terms (the hyperbolic part of the time-dependent Navier-Stokes equations), along with a special treatment of the diffusion terms, provides an appropriate simulation. In order to enable the solution procedure, a time discretization operator has to be utilized as well. Any conventional method, suitable for the

<sup>18</sup> Goldberg U.C., "Prediction of Separated Flows With A New Turbulence Model," *Proceedings of the 5th International Conference on Numerical Methods in Laminar and Turbulent Flow*, Montreal, Quebec, Canada, July 6-10, 1987. (See also *AIAA Journal*, Vol. 26, No. 4, April 1988, pp. 405-408).

<sup>19</sup> Goldberg U.C., "Separated Flow Calculations With A New Turbulence Model," *Proceedings of the First World Congress on Computational Mechanics*, the University of Texas at Austin, September 22-26, 1986.

Navier-Stokes equations, can be used together with the space discretization methodology described above. This includes approximate factorization and relaxation techniques. In recent years, TVD formulations have been constructed for shock-capturing finite-difference methods.<sup>6-9</sup> Near large gradients in the solution (extrema), TVD schemes automatically reduce to first-order accurate discretizations locally, while away from extrema they can be constructed to be of higher-order accuracy. This local effect, which is necessary to prevent the total variation from increasing, restricts the maximum global accuracy possible for TVD schemes to third order for steady-state solutions.

These methods manifest many properties desirable in numerical solution procedures. By design, they avoid numerical oscillations and "expansion shocks" while at the same time being higher-order (more than first-order) accurate. ("Expansion shocks" are shock waves which do not satisfy the entropy inequality). TVD formulations are also based on the principle of discrete or numerical conservation, which is the numerical analog of physical conservation of mass, momentum, and energy. This results in TVD schemes being able to "capture" discontinuities with ease and high resolution. At a fundamental level, they are based on upwind schemes; therefore, they closely simulate the signal propagation properties of hyperbolic equations.

Schemes based on the TVD formulation are completely defined. In other words, the user does not have to specify any "numerical" parameters such as "dissipation coefficients" to be able to carry out the computations. In contrast, central difference schemes involve dissipation terms for stability and have one or more coefficients that must be judiciously chosen to achieve desirable results. Methods based on TVD formulations represent mature CFD technology and are being applied to a wide class of problems.<sup>8</sup>

Proper treatment of the diffusion terms of the Navier-Stokes equations is also important in the construction of reliable numerical methods. Unidirectional second derivative terms are treated by using central difference approximations. Cross derivatives are represented by finite-differences, the nature of which depends upon the sign of the coefficient of such terms. This treatment augments diagonal dominance of the resulting set of discretized equations, without detracting from the accuracy and while adding to the reliability of the numerical procedure. Further details can be found in Reference 6. The diagonal dominance of TVD schemes (with suitable discretized cross derivative terms) makes it possible to use relaxation methods. However, conventional approximate factorization methods are used to solve multidimensional implicit formulations in the present study.

#### 4. COMPUTATIONAL GRID.

The problem of computing internal/external SFRJ projectile flowfields is complicated by the internal geometry involved. As illustrated in Figure 1, the SFRJ consists of several sharp corners that would severely hamper conventional grid generation schemes that require one set of grid lines to be tangent to the surface and another set to be normal to it.<sup>12</sup> The SFRJ geometry is more easily gridded by the zonal approach. The internal geometry of the SFRJ is broken up into four zones of simple geometric shape (Figure 2). In each zone any approach to generating the grid can be used, such as algebraic methods, differential equations methods, etc. In this case a simple algebraic grid is used with grid

clustering near the surface and other regions where high gradients are expected (Figure 3). In the zonal approach, the computational method and computer program are constructed in such a manner that each zone may be considered as an independent module, interacting with each other before or after the information corresponding to each zone is updated one cycle. In addition, the zonal boundaries can be made transparent to flowfield phenomena (e.g. shock waves). The actual grid used for these computations consisted of the following dimensions for zones 1 through 6: 60x61, 7x30, 80x49, 40x30, 15x49, and 45x20. These grid dimensions represent a refinement over a coarse grid that was initially used (30x35, 7x17, 50x30, 30x17, 15x25, 45x20).<sup>3</sup> The computational results were found to be essentially independent of these two grids when all other factors (e.g. flow turbulence and transition modelling) were the same. However, the fine grid was preferred for resolving flow details within boundary layers. The grids have been generated in such a manner that the horizontal families of mesh lines within the projectile are continuous between zones and the vertical families are continuous in the zones external to the SFRJ. While this type of grid is natural for this problem, the computational methodology permits a wider class of patched zonal grids where neither family of grid lines need be continuous across zones.

### III. RESULTS

The computational solutions are compared with internal surface pressure measurements of an inert SFRJ. The model was instrumented with pressure taps and mounted in the Mach 4, nine-inch blowdown tunnel at the NASA Langley Research Center. The details of these tests are described in Reference 14. The freestream Mach number and Reynolds number were 4.03 and about 20 million per foot, respectively. The model was at zero yaw.

In the computational solutions, the freestream Mach number was increased gradually as the numerical iterations progressed. At a given point in the iteration cycle, the Mach number was fixed and the iterations continued until convergence. For the Euler (inviscid) solutions, the Mach number was linearly increased from 0.03 to 4.03 for 3000 iterations and then held fixed for the balance of 5000 total iterations. For the Navier-Stokes solutions, the Mach number was linearly increased from 0.03 to 4.03 for 1000 iterations and then held fixed for the balance of 5000 total iterations. The more conservative treatment for the Euler cases was necessary given the complex geometry of the SFRJ and the lack of natural viscosity to damp transients developing in the inviscid flow. In all cases convergence was determined by the arrival at a time-asymptotic steady-state solution. The CFL number (stability requirement for the numerical solution of hyperbolic partial differential equations) for these results was set at 1.0 for the Euler solutions, and between .5 to 2.5 for the Navier-Stokes solutions, although solutions can be achieved in about 1000 iterations with CFL numbers as high as 10. Typical run times on a Cray XMP 4/8 computer for Euler and Navier-Stokes solutions were 0.8 and 1.2 CPU hours, respectively.

The Navier-Stokes solutions consisted of both laminar and turbulent cases. In the turbulent cases the Baldwin-Lomax model was used both with and without the Goldberg backflow model previously described. For those cases in which the latter model was invoked, it was only used if the computed flow conditions (based on the Baldwin-Lomax

model) indicated flow separation. If this condition did not occur the Baldwin-Lomax model was used exclusively. Due to the zonal nature of the code, a flow type (laminar or turbulent) can be assigned to each zone. In certain solutions all zones were solved with the same flow type assumption.

## 1. IMPORTANCE OF FLOW TRANSITION AND TURBULENCE.

As indicated previously, the present CFD code can be run in several modes. These modes include inviscid, laminar, and turbulent flow and involve the solution of the Euler or the Navier-Stokes equations. For any given geometry and flow conditions, the mechanisms that control transition from laminar to turbulent flow and the presence of attached or detached flow are not completely understood. To achieve reliable results then, the code must be used in several modes. Comparison of the results can indicate the impact of turbulence and flow detachment for a particular configuration. In addition, various flow transition locations can be studied.

Figure 4 shows computed internal wall pressure distributions for the configuration with 1.7 inch injector and 1.6 inch nozzle diameters. The code was run assuming inviscid, laminar, turbulent, and turbulent/detached flow. For the turbulent cases, transition from laminar to turbulent flow was specified near the leading edge of the inlet. The best overall agreement of the computations with pressure data in the combustion section ( $3 \leq x \leq 9$ ) is achieved when the backflow turbulence model is used. In this section, the flow can be characterized as turbulent and detached. Studies of the computed flow velocity vectors indicate that the combustion region is dominated by a separation bubble. Here, the flow separation point is determined by the sharp corner of the injector.

In the inlet ( $0 \leq x < 3$ ) the computations with turbulence predict an expansion at the leading edge, followed by a gradual compression that starts at about one-third the inlet length from the leading edge (i.e. the flow separation point). The Baldwin-Lomax turbulence model predicts the separation point slightly further upstream than the backflow turbulence model of Goldberg. However, the wind tunnel data show a constant pressure over the entire inlet indicating flow separation at or near the leading edge of the inlet. Unexpectedly, the computations assuming laminar flow better match the data in the inlet. This result suggests either; 1) that the inlet flow is turbulent and detached but the Baldwin-Lomax turbulence model and the Goldberg backflow model predict flow separation further downstream than indicated by the wind tunnel data, or 2) that the inlet flow is transitional (i.e. neither fully turbulent nor laminar) and the point of transition from laminar to turbulent flow cannot be arbitrarily specified.

Figure 5 shows the effects of flow transition location on turbulent/detached flow computations for the configuration with 1.7 in. injector and 1.6 in. nozzle diameters. For the two computations shown, flow transition has been specified at either the beginning of the inlet or at the end of the inlet (i.e. at the injector). For the latter case, the inlet flow is computed as laminar and the best overall comparison with wind tunnel data, in this region, is achieved. Studies of the computed flow velocity vectors indicate that a large separation bubble extends over the entire inlet length. The laminar flow assumption more accurately predicts the separation point in the inlet. This result is unexpected since

laminar/separated flows are unusual. However, as stated above the turbulence models employed may be deficient in predicting the flow separation point in the inlet. Specifying transition at the injector improves agreement with data behind the injector but degrades agreement at the end of the combustion section. For the entire configuration, the best overall agreement between computed and measured wall pressures is achieved for injector transition.

Figure 6 shows the results of a similar flow transition study for a configuration with 1.9 in. injector and 1.1 in. nozzle diameters. In contrast to the 1.6 in. nozzle, the smaller nozzle diameter causes a normal shock at the leading edge of the SFRJ with subsonic flow throughout the interior. For this configuration, the best overall agreement with wind tunnel data occurs when flow transition is specified at the beginning of the inlet. In this case, the normal shock has determined the point of flow separation. In summary, the SFRJ configurations studied to date indicate that flow transition may occur at the beginning of the inlet for subsonic cases (nozzle diameter 1.1 in.) and at the end of the inlet for supersonic cases (nozzle diameter 1.6 in.).

## 2. DISCUSSION OF COMPUTED RESULTS.

Figure 7 shows comparisons of internal surface pressure measurements and turbulent/detached flow computations for three SFRJ configurations. The configuration used in SFRJ flight tests (1.7 inch injector and 1.54 inch nozzle diameter) is included. These configurations differ only in the nozzle diameter; 1.6 in., 1.54 in., and 1.1 in. The injector diameter was 1.7 in. in each case. The criterion established in the previous section was used to specify the flow transition location. The lower pressure level for the 1.6 and 1.54 in. nozzle configurations is indicative of supersonic internal flow, with the exception of the wall boundary layers and detached regions. Although obscured by the scale of this plot, the overall agreement between computation and measurements for the smaller nozzle diameters is notably better than that for the 1.1 in. nozzle (see Figure 5). Figure 8 shows the pressure contours for the 1.6 in. nozzle SFRJ. An oblique shock is attached to the leading edge of the SFRJ and intersects the centerline of the model as a normal shock. Examination of the computed velocity vectors shows that the inlet flow is dominated by a separation bubble that terminates at the injector where an oblique shock is generated. The flow in the combustion section is also dominated by a separation bubble that extends from the injector to the nozzle and well into the flowfield. A zero wall pressure gradient extends throughout this region (see Figure 8). Several shock reflections occur throughout the combustion and nozzle sections.

Danberg,<sup>13</sup> used an axisymmetric method of characteristics solution to investigate possible inlet flow patterns. This analysis assumed separated flow over the entire length of the inlet and a constant inlet wall pressure at the experimentally determined pressure level. This calculation showed that an oblique shock emanates from the leading edge of the inlet and terminates in a normal shock at the centerline. Danberg showed that the inlet flow pattern bears a striking resemblance to that of an over-expanded jet (where the jet exit coincides with the inlet entrance).

The higher pressure level for the 1.1 in. nozzle diameter (Figure 7) indicates subsonic

internal flow caused by an expelled leading edge normal shock. The computed wall pressure matches the distribution but not the level of the measured pressure. Indeed the computed pressure level better matches the measured result for the 1.2 in. nozzle (see Figure 10, Reference 3). This would indicate a nozzle wall boundary layer thickness which is predicted to be thinner than the actual one. This could be the result of turbulence model deficiency since these computed pressures were found to be independent of grid resolution normal to the nozzle wall. Investigations with other turbulence models should clarify this point.

Figure 9 shows the pressure contours for the 1.1 in. nozzle SFRJ. A normal shock is clearly seen at the leading edge. Upon detailed examination, the presence of flow spillage to the exterior has been found. The subsonic interior flow expands through the diverging inlet, and the pressure remains relatively constant throughout the combustion section. Expansion back to supersonic flow is accomplished by the nozzle. Examination of the computed velocity vectors shows that the inlet flow separates at about two-thirds of the length from the leading edge. In the combustion section a large separation bubble is established behind the injector that thins to a narrow region of separated flow near the wall of the combustor. In contrast, a larger nozzle diameter (1.6 inches) produces large separated flow regions that dominate both the inlet and the combustion sections.

Figure 10 shows comparisons between internal surface pressure measurements and turbulent/detached flow computations for three SFRJ configurations with an injector diameter of 1.9 in. and nozzle diameters of 1.6 in., 1.54 in., and 1.1 in. The criterion established in the previous section was used to specify the flow transition location. The similarity of these results with those for the 1.7 in. nozzle (Figure 7) indicates the relative insignificance of the injector diameter in determining the internal wall pressures.

#### IV. CONCLUSIONS

Computational solutions of the internal and external flowfield for inert SFRJ projectiles at zero yaw have been performed using a zonal Navier-Stokes code with a TVD scheme. Comparisons between computed and measured internal surface pressures were made.

The flow transition location was guided by measured internal wall pressure data and chosen to achieve the best overall agreement with measured data. While the inlet flow transition point is determined by the expelled normal shock for subsonic internal flow (1.1 inch nozzle diameter), for supersonic flow (1.6 inch nozzle diameter), the transition point location is unclear. The best agreement with measured wall pressures is achieved when flow transition is specified at the end of the inlet (at the injector). The best overall agreement with the measured pressure level and gradient along the combustion section, was achieved using the backflow turbulence model of Goldberg.

The agreement with measured internal wall pressures lends assurance that computed flow predictions can correctly replicate physical flow details. This agreement was achieved with the aid of experimental data to guide the location of flow transition. These computations indicate that nozzle diameters of about 1.6 inches yield a leading edge oblique

shock and supersonic core flow. The inlet and combustion sections are dominated by flow detachment. A nozzle diameter of 1.1 inches yields an expelled leading edge normal shock, subsonic internal flow, and a choked nozzle.

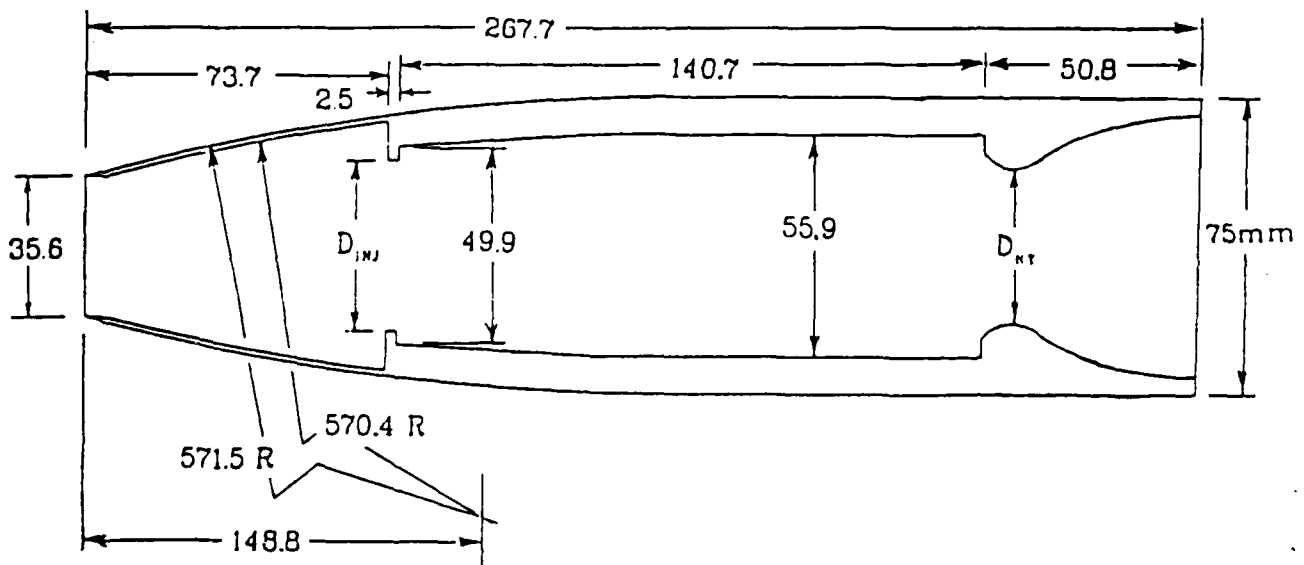
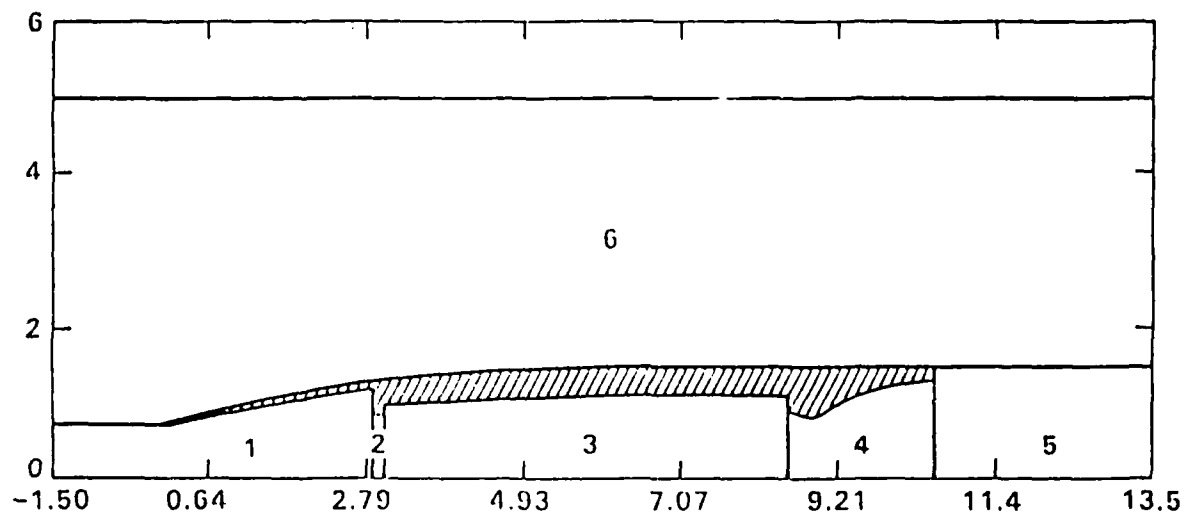
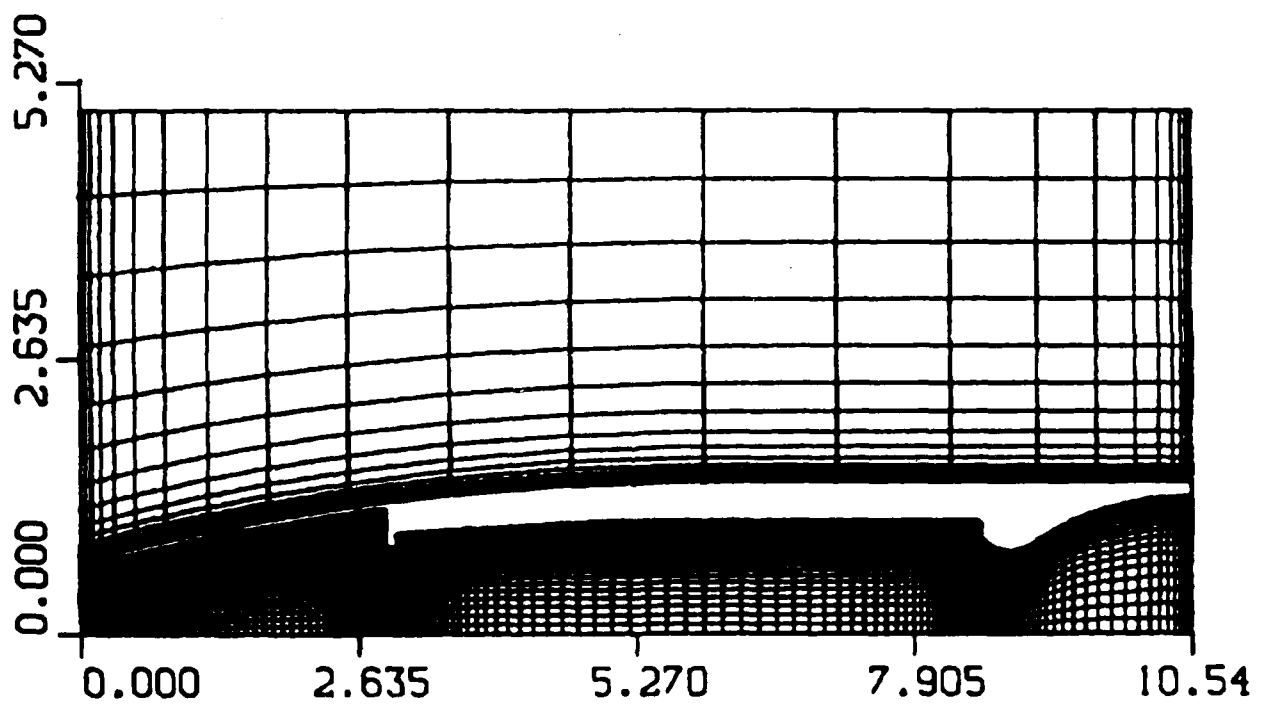


Figure 1. SFRJ Geometry; Dimensions in Millimeters,  $D_{inj}$ =43.2, 48.3mm (1.7, 1.9 Inches),  $D_{nt}$ =27.9, 39.7, 40.6 mm (1.1, 1.564, 1.6 Inches).



**Figure 2.** Zone Designations for Axisymmetric SFRJ Geometry. Dimensions in Inches.  
 1: Inlet; 2: Injector; 3: Combustion Section; 4: Nozzle; 5: Base; 6: Exterior.



**Figure 3.** Computational Grid for Axisymmetric SFRJ. Dimensions in Inches (Nearfield Shown).

Navier-Stokes Computation for SFRJ  
 1.7 in. Injector, 1.6 in. Nozzle  $M_\infty = 4.03$

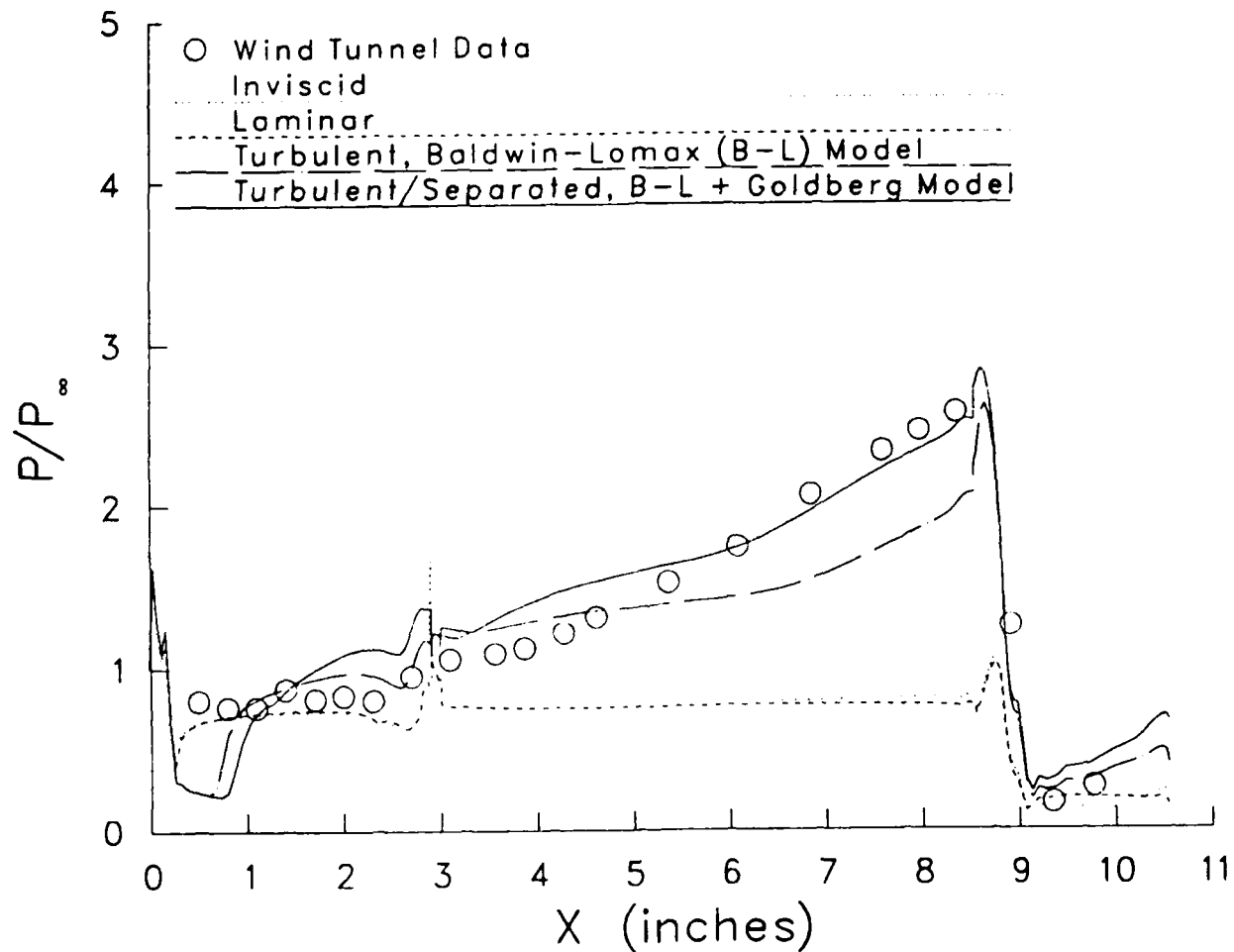
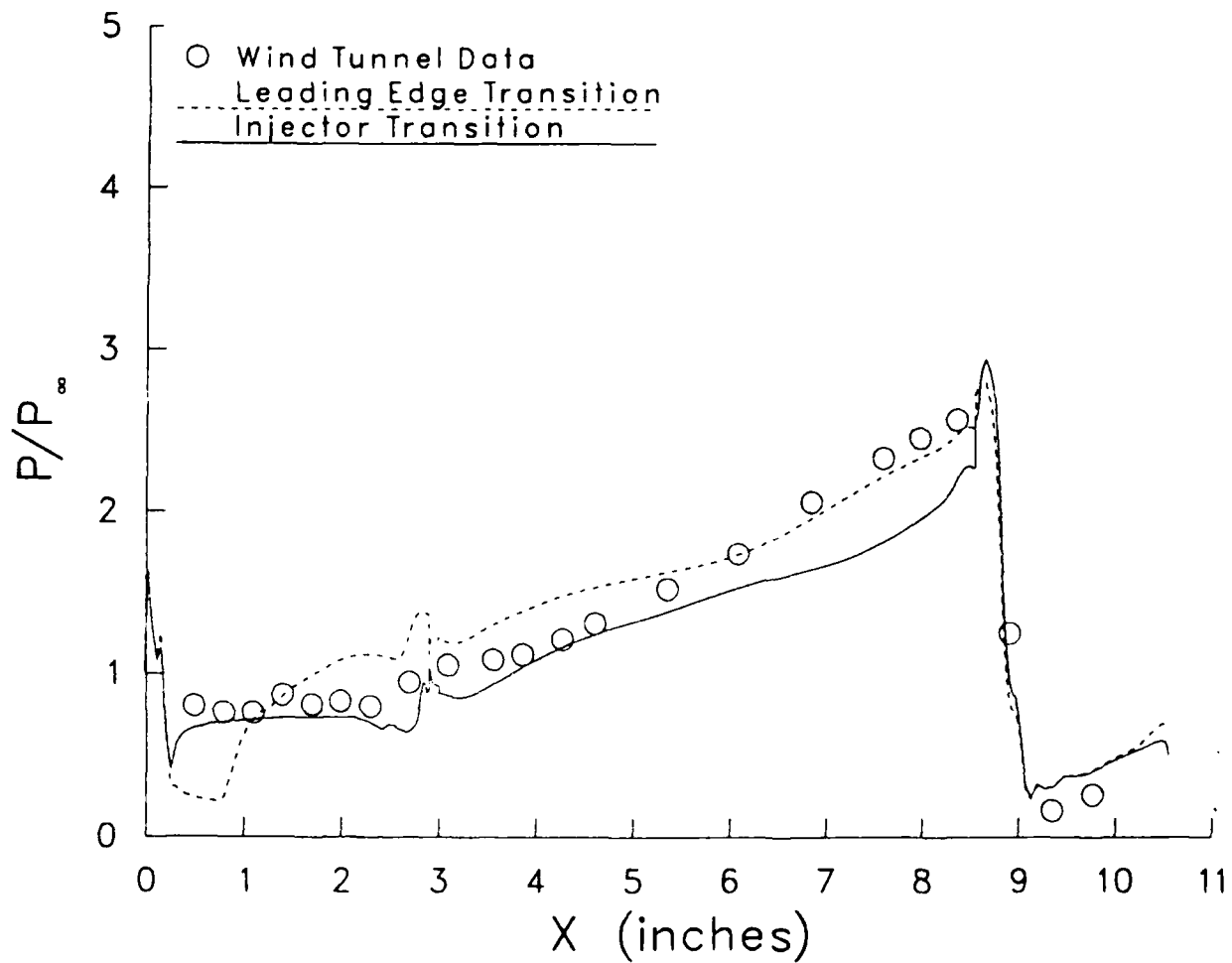


Figure 4. Internal Surface Pressure Distribution for SFRJ,  $M_\infty=4.03$ , 1.7 in. Injector, 1.6 in. Nozzle. Effect of Viscous Modeling.

Navier-Stokes Computation for SFRJ  
1.7 in. Injector, 1.6 in. Nozzle  $M_\infty = 4.03$



**Figure 5.** Internal Surface Pressure Distribution for SFRJ,  $M_\infty=4.03$ , 1.7 in. Injector, 1.6 in. Nozzle. Effect of Flow Transition Location.

Navier-Stokes Computation for SFRJ  
1.9 in. Injector, 1.1 in. Nozzle  $M_\infty = 4.03$

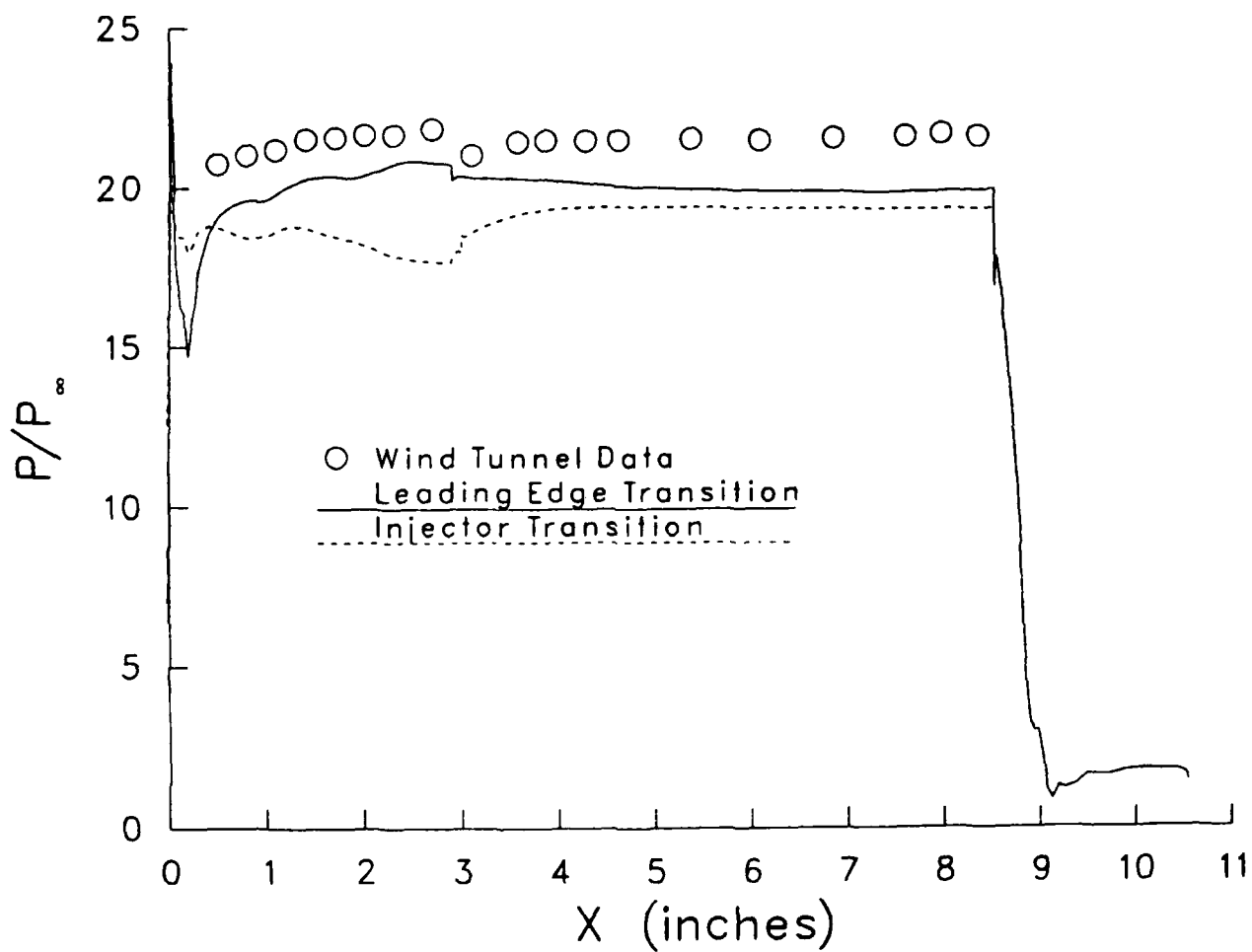
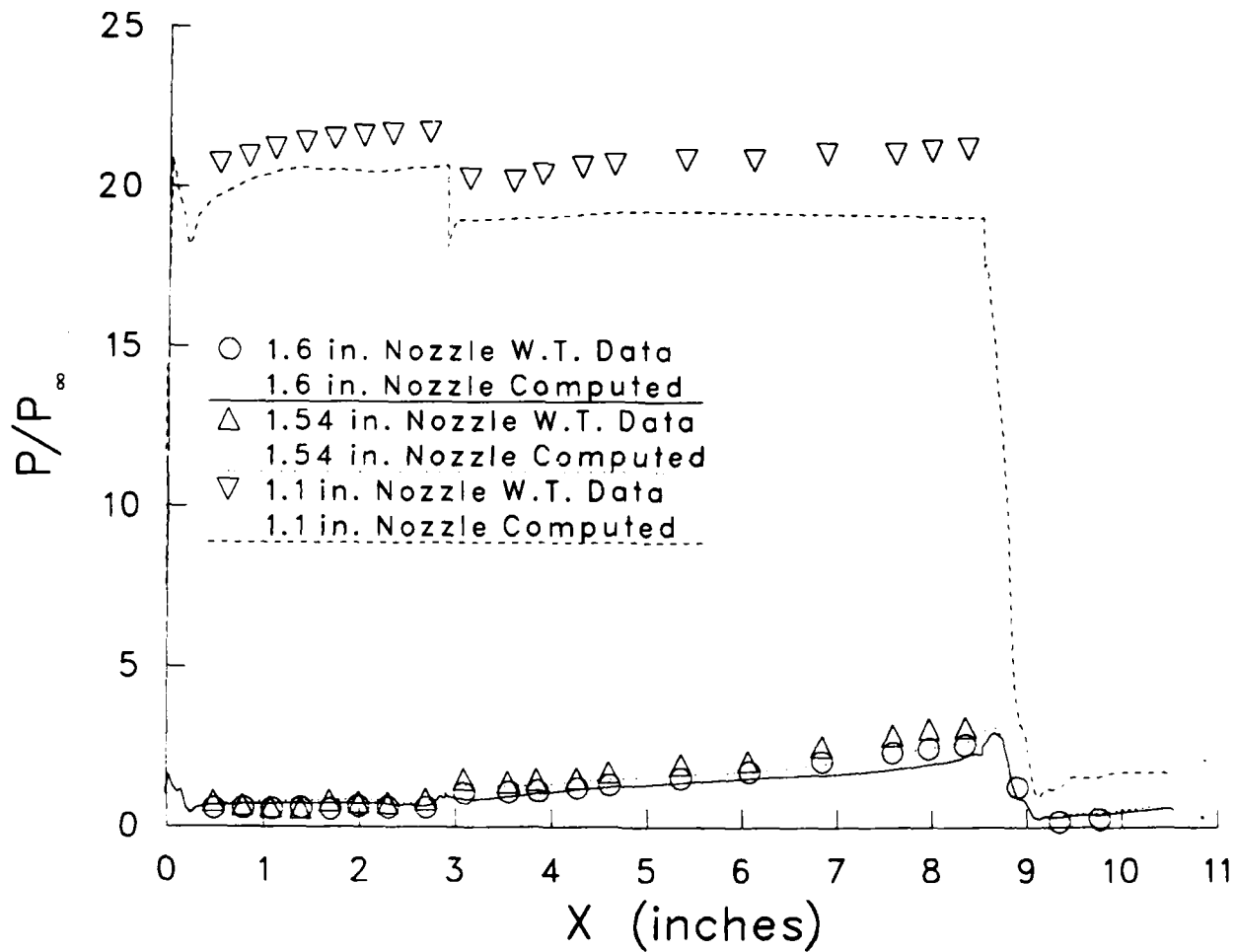
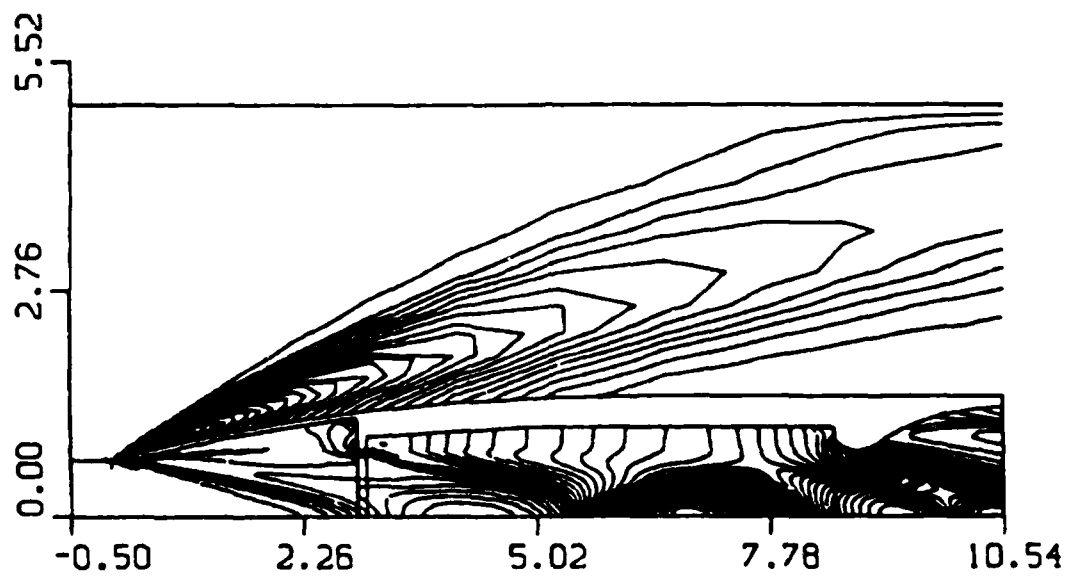


Figure 6. Internal Surface Pressure Distribution for SFRJ,  $M_\infty=4.03$ , 1.9 in. Injector, 1.1 in. Nozzle. Effect of Flow Transition Location.

Navier-Stokes Computation for SFRJ  
1.7 in. Injector  $M_\infty = 4.03$



**Figure 7.** Internal Surface Pressure Distribution for SFRJ,  $M_\infty=4.03$ , 1.7 in. Injector, 1.1, 1.54, and 1.6 in. Nozzles.



**Figure 8.** Pressure Contours for SFRJ,  $M_\infty=4.03$ , 1.7 in. Injector, 1.6 in. Nozzle. Dimensions in Inches.

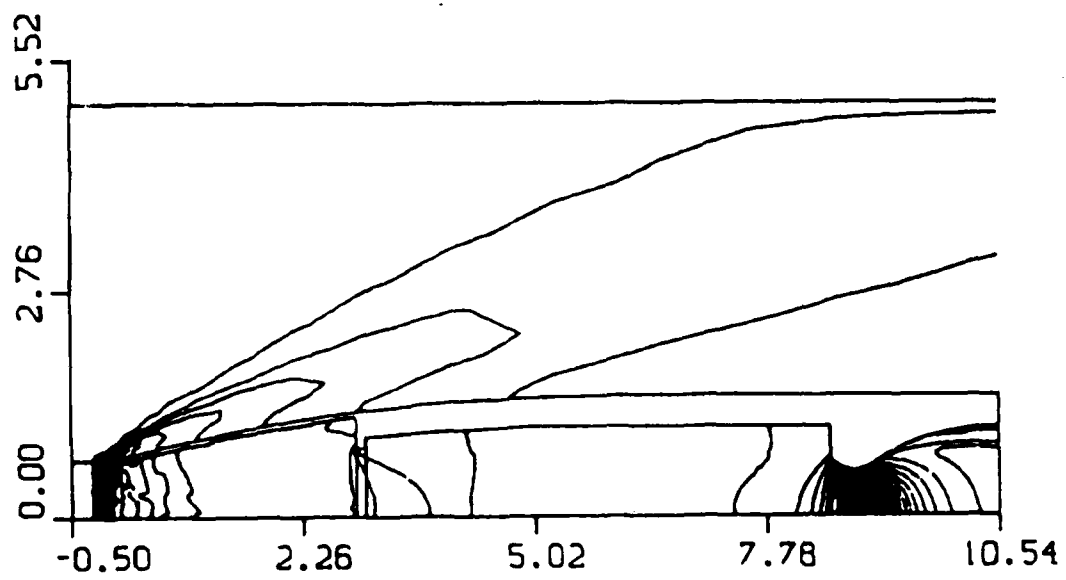


**Figure 9.** Pressure Contours for SFRJ,  $M_\infty=4.03$ , 1.7 in. Injector, 1.1 in. Nozzle. Dimensions in Inches.

Navier-Stokes Computation for SFRJ  
 1.9 in. Injector  $M_\infty = 4.03$

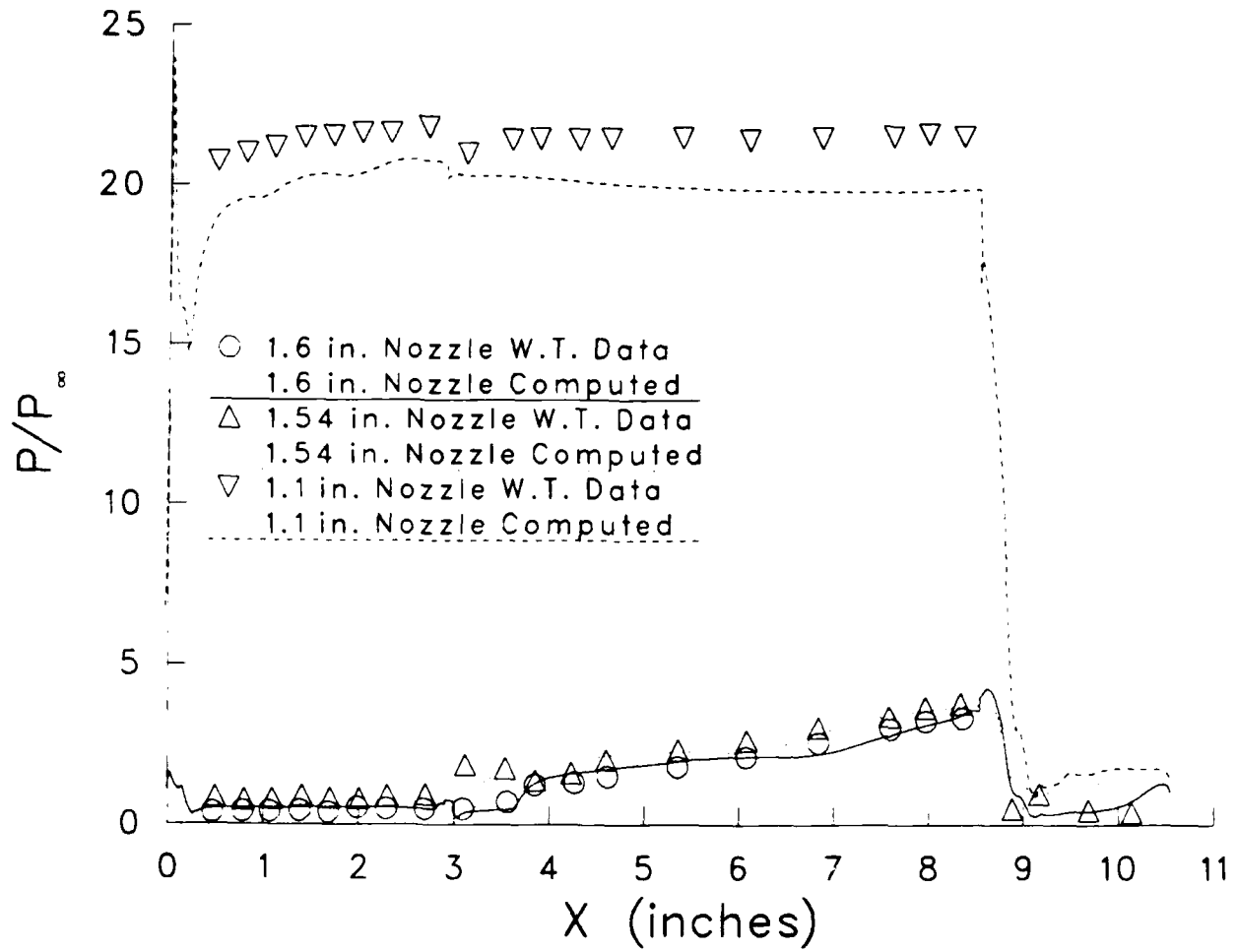


Figure 10. Internal Surface Pressure Distribution for SFRJ,  $M_\infty=4.03$ , 1.9 in. Injector, 1.1, 1.54, and 1.6 in. Nozzles.

## References

1. Mermagen, W.H., Yalamanchili, R.J., "First Diagnostic Tests of a 75mm Solid Fuel Ramjet Tubular Projectile," ARBRL-03283, U.S. Army Ballistic Research Laboratory, Aberdeen Proving Ground, MD, June 1983. (AD A130598)
2. Mermagen, W.H., Yalamanchili, R.J., "Experimental Tests of a 105/75mm Solid Fuel Ramjet Tubular Projectile," ARBRL-MR-3416, U.S. Army Ballistic Research Laboratory, Aberdeen Proving Ground, MD, December 1984. (AD B089766)
3. Chakravarthy, S.R. "A New Computational Capability for Ramjet Projectiles," ARBRL-CR-595, U.S. Army Ballistic Research Laboratory, Aberdeen Proving Ground, MD, March 1988. (Also Goldberg, U., Chakravarthy, S. and Nusca, M., AIAA-87-2411, Proceedings of the 14th AIAA Atmospheric Flight Mechanics Conference, Monterey, CA, August 17-19, 1987.)
4. Baldwin, B.S. and Lomax, H., "Thin Layer Approximation and Algebraic Model for Separated Turbulent Flows," AIAA-78-257, Proceedings of the 16th AIAA Aerospace Sciences Meeting, Huntsville, AL, January 16-18, 1978.
5. Goldberg, U.C., "Separated Flow Treatment with a New Turbulence Model," AIAA Journal, Vol. 24, No. 10, October 1986, pp. 1711-1713.
6. Chakravarthy, S.R., Szema, K.Y., Goldberg, U.C., Gorski, J.J. (Rockwell International Science Center) and Osher, S. (University of California), "Application of a New Class of High Accuracy TVD Schemes to the Navier-Stokes Equations," AIAA-85-0165, Proceedings of the 23rd AIAA Aerospace Sciences Meeting, Reno, NV, January 14-17, 1985.
7. Chakravarthy, S. and Szema, K., "An Euler Solver for Three-Dimensional Supersonic Flows with Subsonic Pockets," AIAA-85-1703, Proceedings of the 18th AIAA Fluid Dynamics and Plasmadynamics and Lasers Conference, Cincinnati, OH, July 16-18, 1985.
8. Chakravarthy, S.R., "The Versatility and Reliability of Euler Solvers Based on High-Accuracy TVD Formulations," AIAA-86-0243, Proceedings of the 24th AIAA Aerospace Sciences Meeting, Reno, NV, January 6-9, 1986.
9. Chakravarthy, S.R., Harten, A. and Osher, S., "Essentially Non-Oscillatory Shock-Capturing Schemes of Arbitrarily-High Accuracy," AIAA-86-0339, Proceedings of the 24th AIAA Aerospace Sciences Meeting, Reno, NV, January 6-9, 1986.
10. Sova, G.J., "Application of Navier-Stokes Analysis to Predict the Internal Performance of Thrust Vectoring Two-Dimensional Convergent-Divergent Nozzles," AIAA-88-2586, Proceedings of the 6th AIAA Applied Aerodynamics Conference, Williamsburg, VA, June 6-8, 1988.
11. Chakravarthy, S.R., Szema, K., and Haney, J.W., "Unified "Nose-to-Tail" Computational Method for Hypersonic Vehicle Applications," AIAA-88-2564. Proceedings of the 6th AIAA Applied Aerodynamics Conference, Williamsburg, VA, June 6-8, 1988.

12. Nietubicz, C.J., and Heavey, K.R., "Computational Flow Field Predictions for Ramjet and Tubular Projectiles," Proceedings of the 8th ADPA International Symposium on Ballistics, Orlando, FL, October 23-25, 1984.
13. Danberg, J.E., and Sigal, A., "Evaluation of Solid Fuel Ramjet Projectile Aerodynamic Characteristics," Proceedings of the 10th ADPA International Symposium on Ballistics, San Diego, CA, October 27-29, 1987.
14. Kayser, L.D., Yalamanchili, R.J. and Trexler, C., "Pressure Measurements on the Interior Surface of a 75mm Tubular Projectile at Mach 4," U.S. Army Ballistic Research Laboratory, Aberdeen Proving Ground, MD, report in preparation.
15. Yalamanchili R.J., unpublished wind tunnel data for the 75mm Tubular Projectile at Mach 4, US Army Ballistic Research Laboratory, Aberdeen Proving Ground, Maryland.
16. Vos, J.B., "Calculating Turbulent Reacting Flows Using Finite Chemical Kinetics," AIAA Journal, Vol. 25, No. 10, October 1987, pp.1365-1372.
17. Mazor, G., Ben-Dor, G. and Igra, O., "A Simple and Accurate Expression for the Viscosity of Nonpolar Diatomic Gases up to 10,000 K," AIAA Journal, Vol. 23, No. 4, April 1985, pp. 636-638.
18. Goldberg, U.C., "Prediction of Separated Flows With A New Turbulence Model," Proceedings of the 5th International Conference on Numerical Methods in Laminar and Turbulent Flow, Montreal, Quebec, Canada, July 6-10, 1987. (See also AIAA Journal, Vol. 26, No. 4, April 1988, pp. 405-408).
19. Goldberg, U.C., "Separated Flow Calculations With A New Turbulence Model," Proceedings of the First World Congress on Computational Mechanics, the University of Texas at Austin, September 22-26, 1986.

DISTRIBUTION LIST

<u>No. of Copies</u>	<u>Organization</u>	<u>No. of Copies</u>	<u>Organization</u>
12	Administrator Defense Technical Info Center ATTN: DTIC-DDA Cameron Station Alexandria, VA 22304-6145	3	Commander Armament RD&E Center US Army AMCCOM ATTN: SMCAR-AET-A (R. Kline) SMCAR-FSP-A (F. Scerbo) SMCAR-FSP-A (J. Bera) Picatinny Arsenal, NJ 07806-5000
1	HQDA (SARD-TR) Washington, DC 20310	1	OPM Nuclear ATTN: AMCPM-NUC (COL W. P. Farmer) Dover, NJ 07801-5001
1	Commander US Army Materiel Command ATTN: AMCDRA-ST 5001 Eisenhower Avenue Alexandria, VA 22333-0001	1	Director Benet Weapons Laboratory Armament R&D Center US Army AMCCOM ATTN: SMCAR-LCB-TL Watervliet, NY 12189
1	Commander US Army Laboratory Command ATTN: AMSLC-TD Adelphi, MD 20783-1145	1	Commander US Army Armament, Munitions and Chemical Command ATTN: SMCAR-ESP-L Rock Island, IL 61299
1	Commander Armament RD&E Center US Army AMCCOM ATTN: SMCAR-MSI Picatinny Arsenal, NJ 07806-5000	1	Commander US Army Aviation Systems Command ATTN: AMSAV-DACL 4300 Goodfellow Blvd. St. Louis, MO 63120
1	Commander Armament RD&E Center US Army AMCCOM ATTN: SMCAR-TDC Picatinny Arsenal, NJ 07806-5000	1	Director US Army Aviation Research and Technology Activity Ames Research Center Moffett Field, CA 94035-1099
1	Commander Armament RD&E Center US Army AMCCOM ATTN: SMCAR-CAWS-AM (Mr. DellaTerga) Picatinny Arsenal, NJ 07806-5000	1	Commander US Army Communications - Electronics Command ATTN: AMSEL-ED Fort Monmouth, NJ 07703
		1	Commander US Army Missile Command ATTN: AMSMI-RD Redstone Arsenal, AL 35898-5000

DISTRIBUTION LIST

<u>No. of Copies</u>	<u>Organization</u>	<u>No. of Copies</u>	<u>Organization</u>
1	Commander US Army Missile Command ATTN: AMSMI-AS Redstone Arsenal, AL 35898-5000	1	Commander Naval Surface Weapons Center ATTN: Dr. W. Yanta Aerodynamics Branch K-24, Bldg. 402-12 White Oak Laboratory Silver Spring, MD 20910
1	Commander US Army Missile Command ATTN: AMSMI-RDK (Mr. Dahlke) Redstone Arsenal, AL 35898-5000	1	Air Force Armament Laboratory ATTN: AFATL/DLODL Eglin AFB, FL 32542-5000
1	Commander US Army Tank Automotive Command ATTN: AMSTA-DI Warren, MI 48090	1	Commander Defense Advanced Research Projects Agency ATTN: MAJ R. Lundberg 1400 Wilson Blvd. Arlington, VA 22209
1	Director US Army TRADOC Analysis Command ATTN: ATAA-SL White Sands Missile Range NM 88002	1	Director Lawrence Livermore National Laboratory ATTN: Mail Code L-35 (Mr. T. Morgan) P.O. Box 808 Livermore, CA 94550
1	Commandant US Army Infantry School ATTN: ATSI-CD-CSO-OR Fort Benning, GA 31905	1	Director Sandia National Laboratories ATTN: Dr. W. Oberkamp Dr. W. P. Wolfe Division 1636 Albuquerque, NM 87185
1	AFWL/SUL Kirtland AFB, NM 87117	2	Director National Aeronautics and Space Administration Langley Research Center ATTN: Technical Library Langley Station Hampton, VA 23365
1	Commander US Army Dugway Proving Ground ATTN: STEDP-MI (G. C. Travers) Dugway, UT 84022	1	Director National Aeronautics and Space Administration Marshall Space Flight Center ATTN: Dr. W. W. Fowlis Huntsville, AL 35812
1	Commander US Army Yuma Proving Ground ATTN: STEYP-MTW Yuma, AZ 85365-9103		
1	Commandant US Army Field Artillery School ATTN: ATSF-GD Fort Sills, OK 73503		
1	Director US Army Field Artillery Board ATTN: ATZR-BDW Fort Sills, OK 73503		

DISTRIBUTION LIST

<u>No. of Copies</u>	<u>Organization</u>	<u>No. of Copies</u>	<u>Organization</u>
1	Director National Aeronautics and Space Administration Ames Research Center ATTN: Dr. J. Steger Moffett Field, CA 94035	1	Arizona State University Department of Mechanical and Energy Systems Engineering ATTN: Dr. G.P. Neitzel Tempe, AZ 85281
1	Aerospace Corporation Aero-Engineering Subdivision ATTN: Walter F. Reddall El Segundo, CA 90245	1	Director Johns Hopkins University Applied Physics Laboratory ATTN: Dr. Fred Billig John Hopkins Road Laurel, MD 20707
1	Calspan Corporation ATTN: W. Rae P.O. Box 400 Buffalo, NY 14225	1	Massachusetts Institute of Technology ATTN: H. Greenspan 77 Massachusetts Avenue Cambridge, MA 02139
1	Hughes Aircraft ATTN: Dr. John McIntyre Mail Code S41/B323 P.O. Box 92919 Los Angeles, CA 90009	1	North Carolina State University Mechanical and Aerospace Engineering Department ATTN: F. F. DeJarnette Raleigh, NC 27607
1	Interferometrics, Inc. ATTN: Mr. R. F. L'Arriva 8150 Leesburg Pike Vienna, VA 22180	1	Northwestern University Department of Engineering Science and Applied Mathematics ATTN: Dr. S. H. Davis Evanston, IL 60201
3	Rockwell International Science Center ATTN: Dr. V. Shankar Dr. S. Chakravarthy Dr. U. Goldberg 1049 Camino Dos Rios P.O. Box 1085 Thousand Oaks, CA 91360	1	Renssalaer Polytechnic Institute Department of Math Sciences Troy, NY 12181
2	United Technologies Corporation Chemical Systems Division ATTN: Dr. R. O. MacLaren Mr. A. L. Holzman 600 Metcalf Road, P.O. Box 50015 San Jose, CA 95150-0015	1	University of California - Davis ATTN: Dr. Harry A. Dwyer Davis, CA 95616
		1	University of Colorado Department of Astro-Geophysics ATTN: E. R. Benton Boulder, CO 80302

DISTRIBUTION LIST

<u>No. of Copies</u>	<u>Organization</u>	<u>No. of Copies</u>	<u>Organization</u>
1	University of Delaware Spencer Laboratory Department of Mechanical Engineering ATTN: Prof. Leonard W. Schwartz Newark, DE 19716		<u>Aberdeen Proving Ground</u>  Director, USAMSA ATTN: AMXS-D AMXS-MP, H. Cohen AMXS-RA, R. Scungio
2	University of Maryland ATTN: W. Melnik J. D. Anderson College Park, MD 20740		Commander, USATECOM ATTN: AMSTE-TO-F AMSTE-TE-F, W. Vomocil
1	University of Maryland Baltimore County Department of Mathematics ATTN: Dr. Y. M. Lynn 5401 Wilkens Avenue Baltimore, MD 21228		PM-SMOKE, Bldg. 324 ATTN: AMCPM-SMK-M J. Callahan  Commander, CRDEC, AMCCOM ATTN: SMCCR-RSP-A M.C. Miller D. Olson SMCCR-MU W. Dee C. Hughes D. Bromley SMCCR-SPS-IL

USER EVALUATION SHEET/CHANGE OF ADDRESS

This laboratory undertakes a continuing effort to improve the quality of the reports it publishes. Your comments/answers below will aid us in our efforts.

- 1. Does this report satisfy a need? (Comment on purpose, related project, or other area of interest for which the report will be used.) \_\_\_\_\_
- 2. How, specifically, is the report being used? (Information source, design data, procedure, source of ideas, etc.) \_\_\_\_\_
- 3. Has the information in this report led to any quantitative savings as far as man-hours or dollars saved, operating costs avoided, or efficiencies achieved, etc? If so, please elaborate. \_\_\_\_\_
- 4. General Comments. What do you think should be changed to improve future reports? (Indicate changes to organization, technical content, format, etc.) \_\_\_\_\_

BRL Report Number \_\_\_\_\_ Division Symbol \_\_\_\_\_

Check here if desire to be removed from distribution list. \_\_\_\_\_

Check here for address change. \_\_\_\_\_

Current address: Organization \_\_\_\_\_  
Address \_\_\_\_\_

-----FOLD AND TAPE CLOSED-----

Director  
U.S. Army Ballistic Research Laboratory  
ATTN: SLCBR-DD-T (NEI)  
Aberdeen Proving Ground, MD 21005-5066

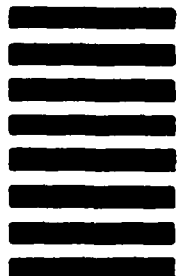
OFFICIAL BUSINESS  
PENALTY FOR PRIVATE USE \$300



NO POSTAGE  
NECESSARY  
IF MAILED  
IN THE  
UNITED STATES

**BUSINESS REPLY LABEL**  
FIRST CLASS PERMIT NO. 12062 WASHINGTON D.C.

POSTAGE WILL BE PAID BY DEPARTMENT OF THE ARMY



Director  
U.S. Army Ballistic Research Laboratory  
ATTN: SLCBR-DD-T (NEI)  
Aberdeen Proving Ground, MD 21005-9989